Applied Ocean Research 65 (2017) 35–46

Contents lists available at ScienceDirect

Applied Ocean Research

journal homepage: www.elsevier.com/locate/apor

Full length article

Hydrodynamic assessment of planing hulls using overset grids

Omer Faruk Sukas, Omer Kemal Kinaci*, Ferdi Cakici, Metin Kemal Gokce

Yildiz Technical University, Naval Architecture and Maritime Faculty, Istanbul, Turkey

ARTICLE INFO

Article history:
Received 6 January 2016
Received in revised form 27 January 2017
Accepted 25 March 2017

Keywords:
Planing hull
Overset grid
Savitsky
Ship resistance
Squat
Hydrodynamic lift
URANS

ABSTRACT

In conjunction with high performance computers, recent developments in computational science paved the path to more accurate representation of body motions inside fluids. Small motions inside the flow can be computationally approximated by using rigid body motion but it is incapable of accurately predicting the large motions of a planing vessel. The implementation of overset grid has made it possible to better approximate the complex fluid-structure interaction problem of the planing regime. The focus of this study was to evaluate the opportunity of using an overset grid system to numerically solve the flow around a planing hull and to understand the planing regime with this invaluable tool. It was shown in this study that the overset grid better captures the large motions of the planing hull at high Froude numbers. Then, the results obtained by overset grid were used to calculate the resistance components of a planing hull in a wide Froude number range. The resistance components were discussed with respect to values generated by Savitsky approach. Using the benefits that the computational science brings, the flow was visualized to explain some underlying physics relevant to the planing regime.

1. Introduction

Planing hulls have been one of the most challenging problems for the naval architecture society as the large motions of the hull complicate hydrodynamical calculations and hull optimization. Researchers have tried to approach the problem experimentally or computationally, though with many assumptions. The large motions of the hull created problems generalizing the experimentally or computationally derived results. It was Savitsky [15] who was one of the first (but definitely the most famous) who succeeded to formulate and generalize the motions of the hull (trim) and the drag (total resistance) it encounters in the flow. There are many studies that came after his. Some tried to formulate the pressure of the underwater hull to calculate slamming effects [13]; others tried to enhance Savitsky's method by introducing whisker spray drag [16] or estimated the wake profile at the aft of the hull [17] to understand the underlying hydrodynamics behind planing regime. But these studies were all empirical approaches to the planing hull problem. They are all valid in a limited range as advised by the researchers who performed the experiments and compiled the results. None of these empirical approaches cover the whole aspects of the flow around a planing hull. If a designer wanted to work with an unconventional planing hull geometry in a Froude (*Fr*) number that is not covered by these works, the remaining options were to conduct experiments or approach the problem with computational fluid dynamics (CFD). Experiments are not economically feasible to do hull optimization of a planing hull as the costs of conducting experiments are substantially higher than approaching the problem computationally. Plus, high speed computers started becoming widespread and the costs of computational methods gradually decreased in the last few decades. Together with commercially available softwares or other in-house codes that are capable of solving viscous flow involving fluid-structure interaction, it has become possible to solve the complicated flow around a planing hull even for the most non-traditional geometries with high accuracy.

There are many computational approaches to hydrodynamically solve the planing hull problem but in general, all of these methods can be classified into two. Likes of Ghassemi [9,6,8] and Matveev [11,12] implement potential theory to solve the inviscid flow around the planing hull and obtain faster results, owing to the practicality of boundary element methods. Stern [14,21] and many others [10,20] use Unsteady Reynolds-Averaged Navier Stokes Equations (URANS) to solve the viscous and transient flow which consumes considerably higher amount of time. In his book *Hydrodynamics of High Speed Marine Vehicles*, Faltinsen [24] broadly covers the literature and explains many flow aspects of planing vessels. In their review article, Yousefi et al. [23] mention the anal-

Abbreviations: URANS, unsteady Reynolds averaged navier stokes; CFD, computational fluid dynamics; DOF, degree of freedom; DFBI, dynamic fluid body interaction; LCG, longitudinal center of gravity; VOF, volume of fluid.

* Corresponding author.
E-mail address: kinaci@yildiz.edu.tr (O.K. Kinaci).

http://dx.doi.org/10.1016/j.apor.2017.03.015
0141-1187/

Nomenclature

B	Breadth of the vessel
C	Courant number
C_F	Frictional resistance coefficient
C_{L0}	Lift coefficient of flat plate
$C_{L\beta}$	Lift coefficient with a deadrise angle
C_Δ	Displacement coefficient
Fr	Froude number
Fr_B	Froude number based on breadth
g	Gravitational acceleration
L_{hd}	Hydrodynamic lift
L_{hs}	Hydrostatic lift
l_p	Center of hydrodynamic pressure
R_F	Frictional resistance
R_P	Pressure resistance
Rn	Reynolds number
S	Sinkage
V_l	Local velocity
V_f	Freestream velocity
V_B	Bottom velocity
β	Deadrise angle
θ	Dynamic trim angle
λ_W	Mean length-to-beam ratio
ν	Kinematic viscosity

ysis techniques of planing hulls referring to many numerical and experimental studies in the literature.

Planing hulls operate at high Froude numbers where the effects of cavitation are likely to occur and disturb the flow. In this study, cavitation effects were not included in the numerical approach. Boundary element methods are handy to solve the flow around cavitating bodies. Bal has selected works on cavitating bodies inside the fluid at high speeds. A numerical model is given in [1] for cavitating hydrofoils. Very high-speed surface-piercing hydrofoils were investigated in [2].

This study covers a thorough discussion on an example planing hull and its resistance components with experimentally, numerically and empirically generated results. The results obtained numerically by implementing overset grid and rigid body motion system in the fluid domain were compared with experiments and Savitsky's empirical approach. Shortcomings of the empirical approach and numerical methods were explained with respect to the experimental data. After validation of numerical methods with a benchmark Fridsma hull, the resistance characteristics of the example planing hull were investigated. Underlying physics of the planing regime were tried to be revealed with the help of computational visualization.

2. Experimental and numerical approach

2.1. Hydrostatics of the hull

A 1/9 scaled model of a prototype hull with a length of 13.374 m hull was numerically and experimentally investigated in this study. Different views of the model can be seen in Fig. 1. The hydrostatic and geometric properties of the hull are given in Table 1.

2.2. Experimental procedure

All towing tests of the model planing hull were performed in the Ata Nutku Ship Model Laboratory of Istanbul Technical University (ITU). The capabilities of the towing tank and its main dimensions are given in Table 2.

Table 1
Hydrostatic and geometric properties of the model planing hull.

	Model Scale: $\lambda = 1/9$		
Length between perpendiculars	L_{BP}	m	1.4860
Maximum breadth	B	m	0.4405
Draft	T	m	0.0844
Displacement volume	∇	m^3	0.0234
Wetted area	S	m^2	0.5718
Block coefficient	C_B	–	0.4170
Longitudinal center of gravity	LCG	m	0.5390
Kinematic viscosity	ν	m^2/s	$1.202 * 10^{-6}$
Density	ρ	kg/m^3	999.6

The towing tank facility has a manned carriage that speeds up to 6 m/s manually. It is equipped with a force dynamometer to measure resistance (X and Y force) and also a computer with some connection equipment for data acquisition.

Tests were performed in calm water and effect of wind resistance is included but not separately calculated in the experiments. For trim and sinkage measurements the model was towed with two free degrees of freedom (2DOF), namely heave and pitch. A 2DOF force dynamometer was mounted between the model and tow post. The tow post was attached to the model at its longitudinal centre of gravity. Values of sinkage and dynamic trim angle were tracked with the help of a laser range finder. All data signals were acquired using a data logger at a certain sample rate and saved on a laptop.

The planing hull was manufactured from wood and scaled by 1/9 to model. The model was towed in calm water at speeds ranging from 0.7 to 5.5 m/s. At the end of the runs, beaches in the towing tank were manually lowered to calm the water. Approximately 15 min of waiting time between two consecutive runs was obligatory to dampen the waves generated during the experiments. The waiting time might be extended up to 1 h to make sure that there were no reflecting waves from the side walls of the tank. Special attention was paid to calibration and misalignment of the dynamometer. The tests were repeated at least 3 times. In spite of all these precautions taken to guarantee high quality test results; if there was a mismatch in integral variables such as resistance, sinkage or trim between the sets, the experiments were repeated 3 more times at least.

2.3. Numerical implementation

A commercial software Star CCM+ was used in this study to model the hydrodynamics of the planing hull. An implicit unsteady solver was selected implementing URANS with k–ε turbulence model. The two-phase flow involving air and water was solved using the Volume of Fluid (VOF) approach that tracks the free surface boundary. The dynamic fluid-body interaction (DFBI) model in the code was activated to have 2DOF for the hull. The planing vessel was free to heave and pitch as in experiments. Time step size was selected according to the instructions set by (ITTC 7.5-03-02-03). The time step sizes used in numerical calculations at each Fr are given in Fig. 2.

Ship motions in the fluid domain were represented using rigid body motion and overset grid systems. The grid was discretized with respect to CFL condition for the highest Froude number and

Table 2
Properties of the Ata Nutku Ship Model Laboratory in ITU.

Length of the channel	m	160
Width of the channel	m	6
Depth of the channel	m	3.4
Max towing speed	m/s	6
Max model length	m	5

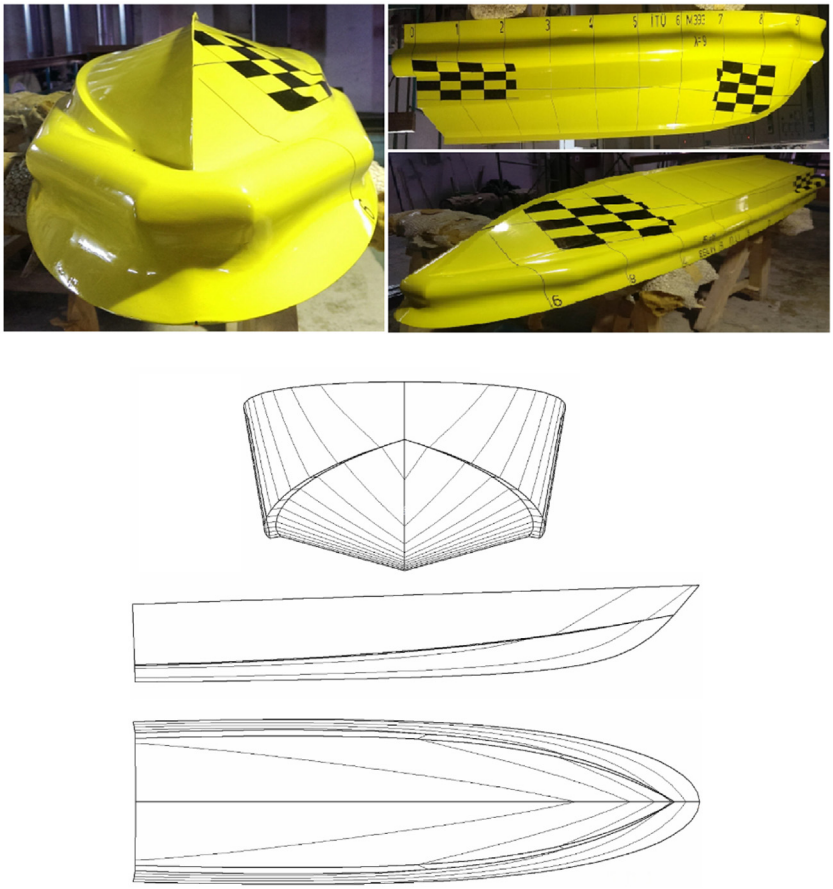

Fig. 1. Different views of the manufactured model for experiments [3] and the basic hull lines of the geometry of the planing hull. The pictures are not to scale.

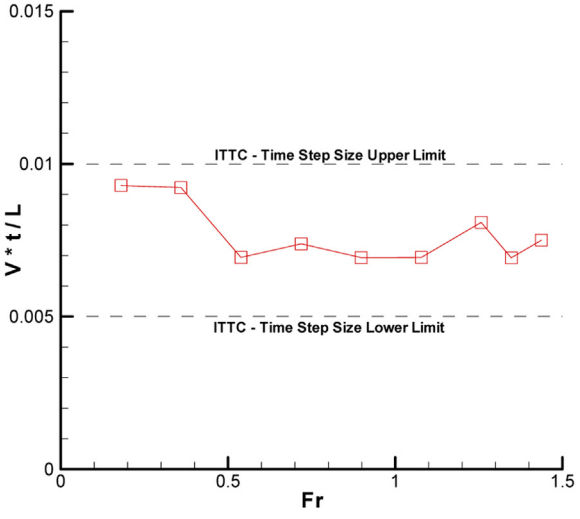

Fig. 2. Selected time step size at each *Fr* in comparison with ITTC limits.

same grids were used throughout the study. As known, CFL condition is:

$$C = \frac{V_i \cdot \Delta t}{\Delta x_i} \leq C_{\max}$$

where Δx is the distance of the first cell to the hull surface and C is the Courant number. To keep values of C close for each numerical simulation, time step size was modified which is a more practical and time saving way of doing computations. Implicit solver was used in this study and therefore the numerical results were less sensitive to the values of $C_{\max}$ where this parameter is taken to be equal to one in explicit solvers. So slight changes in the ratio of $\Delta t/\Delta x_i$ could be tolerated with respect to the changes in the Froude number which depend on the velocity V.

A coarse mesh system to allow better visualization of the elements for the overset grid is given in Fig. 3. In the overset grid system, overlapping elements were used and there were no element deformations. An overlapping grid block that surrounds the planing hull was put on top of a background grid and this block moves together with the motion of the vessel. The overset cell information is given in Fig. 4. For the systematic comparison between the rigid body motion and overset grid systems, the number of elements in the fluid domain was conserved. The details of the overset grid system will not be given here; it can be found in [19]. However, some advantages and the working principle of the overset grid will be briefly explained to express the suitability of this grid system to solve the complex flow around planing hulls.

Overset grid is useful when dealing with moving bodies involving fluid-structure interaction. With this grid implementation, mesh modification or deformation is not necessary which provides great flexibility over the standard meshing techniques. Conservation of cell quality that should be considered at each time step is not an issue in overset grids while this is one of the drawbacks of the deforming grids when there are large motions of the body inside the flow. In overset grid problems, there are a minimum of two regions. One of them is the background region enclosing the whole computational domain and the other is a smaller region which contains the moving body. Cells are grouped into active and inactive cells in this method. Transport equations are only solved for active

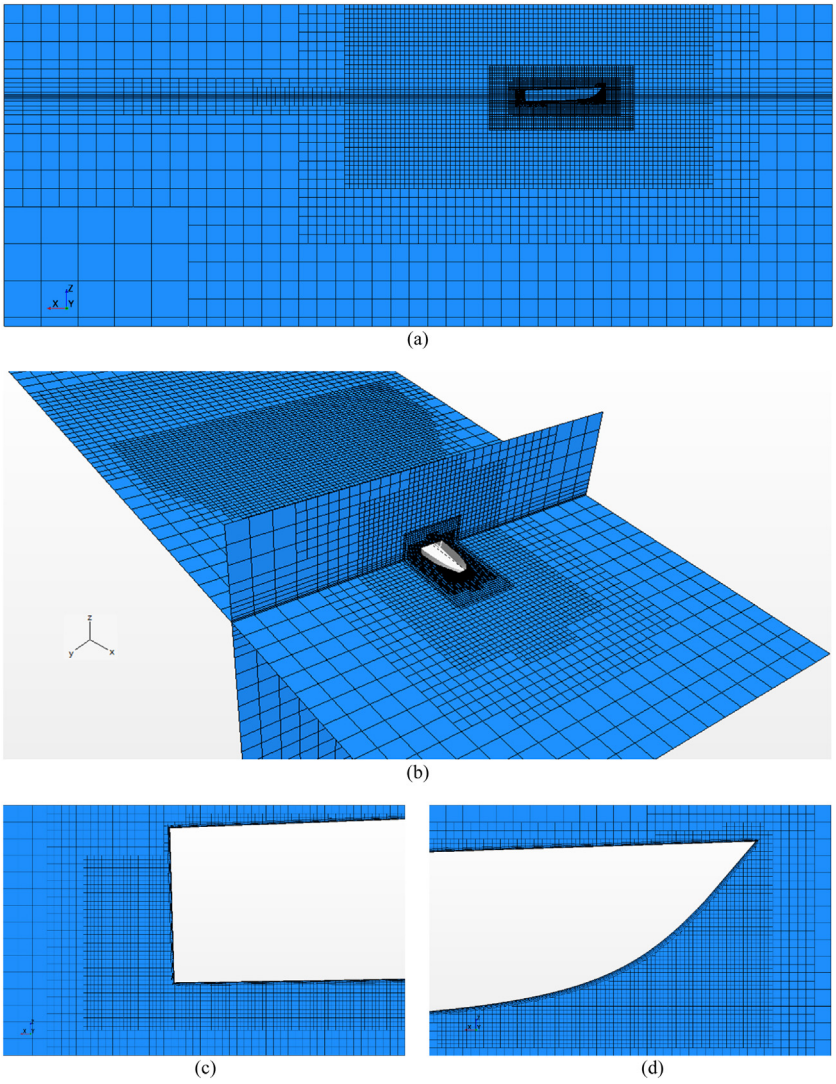

Fig. 3. Example grid system around the planing hull. (a) Overset mesh on top of the background mesh. (b) *xy* and *yz* planes. (c) Refinements near the stern. (d) Refinements near the bow.

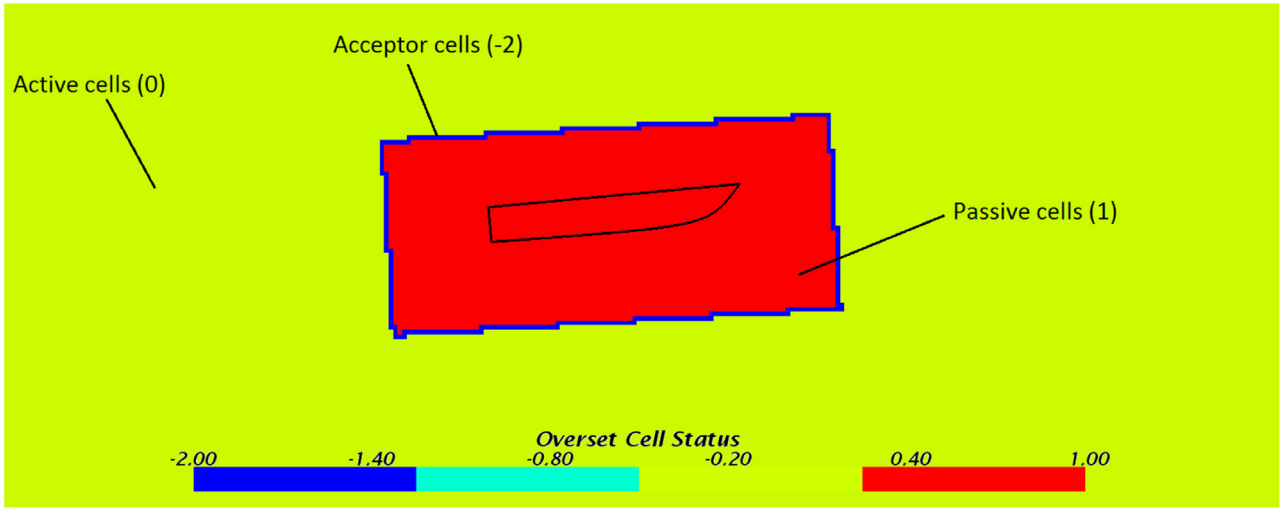

Fig. 4. Overset cell information.

cells while inactive cells are not considered. Acceptor cells separating active and passive cells in the background region lie between the two regions which is used to couple solutions on the two overlapping grids. Information passes from the active cells of one mesh to the active cells of the other through the acceptor cells. Acceptor cells accept values from the other region via interpolation of donor cell values. On the contrary to the flexibility it has, current application of the overset mesh algorithm has some limitations. The most important drawback is that conservation of mass is not strictly imposed with the current interface treatment. However the error is on the order of 0.1% which does not affect the solution to the first 3–4 significant digits (Star CCM+ – User Guide).

2.4. Savitsky method

Savitsky carried out one of the most famous research investigations on planing hulls in 1964. Some mathematical approaches for frictional and pressure resistance, trim angle and some other hydrodynamic parameters based on an extensive number of experiments were done for the first time in his study. His method takes into consideration the hydrostatic and hydrodynamic forces both. Eqs. (1)–(3) were proposed by Savitsky [15]:

$$C_{L\beta} = C_{L0} - 0.0065\beta C_{LO}^{0.6} \tag{1}$$

$$C_{L0} = \theta^{1.1}\left(0.012\lambda_W^{0.5} + 0.0055\frac{\lambda_W^{2.5}}{Fr_B^2}\right) \tag{2}$$

$$\left(\frac{l_p}{\lambda_W B}\right) = 0.75 - \frac{1}{\left(\frac{5.21 Fr_B^2}{\lambda_W^2}\right) + 2.39} \tag{3}$$

Here; β is the deadrise angle, C_{L0} is the lift coefficient when $\beta = 0$, $C_{L\beta}$ is the lift coefficient for a given deadrise angle, B is the breadth of the vessel, Fr_B is the Froude number based on breadth, θ is the dynamic trim angle, l_p is the center of hydrodynamic pressure and λ_W is the aspect ratio. An iterative solution of the above equations solve for C_{L0}, θ and λ_w. The total resistance of the planing hull is given as:

$$R_T = W\tan\theta + \frac{0.5pV_B{}^2\lambda_W B^2 C_F}{\cos\theta\cos\beta} \tag{4}$$

where C_F is the friction coefficient which can approximately be found from of Schoenherr's empirical formula given as:

$$C_F = \left[\frac{0.242}{\log_{10}(Rn\cdot C_F)}\right]^2 \tag{5}$$

$$Rn = V_B\lambda_W B/\nu \tag{6}$$

Eq. (4) calculates the total resistance of the hull and the first term in that equation stands for the pressure resistance while the second term represents the viscous resistance.

$$R_P = W\tan\theta \tag{7}$$

$$R_F = \frac{0.5pV_B{}^2\lambda_W B^2 C_{F0}}{\cos\theta\cos\beta} \tag{8}$$

Details of Savitsky method can be found in his article [15].

3. CFD verification and validation

Before moving on to present the generated results, computational approach was first put to test by performing a numerical convergence analysis for the overset grid system. Three grid types were used to do CFD verification with the overset grid system as established in [18,22]. The total resistance coefficient of the bare hull was taken at $Fr = 1.347$ as the integral variable of the verification. The element numbers in these grids were deviated slightly less than conventionally used Richardson extrapolation technique due to high number of elements demanded by the overset grid. The properties and the generated results for different grid types are provided in Table 3. The iterative uncertainties were very small compared to the grid uncertainties therefore the total numerical uncertainty U_N in this study is given as

Table 3
Grid properties and their uncertainties.

Elements	Grid 3	Grid 2	Grid 1
	2,580k	4,131k	7,405k
S_U	5.841E-03	5.314E-03	5.053E-03
S_L	5.834E-03	5.297E-03	5.019E-03
S_G	5.837E-03	5.306E-03	5.036E-03
U_I	3.314E-06	8.772E-06	1.679E-05

$$U_N = U_G + U_T \tag{9}$$

Here, U_G refers to grid and U_T refers to time step uncertainties. All three cases have achieved oscillatory iterative convergence; therefore, the iterative uncertainty U_I was calculated as

$$U_I = \frac{1}{2}|S_U - S_L| \tag{10}$$

In Table 3, S_U and S_L refer to the upper and lower values of total resistance in the simulations respectively. S_G was calculated as

$$S_G = \frac{1}{2}|S_U + S_L| \tag{11}$$

By taking into account these three grids, the grid uncertainty and grid correction factor as proposed in [18,22] were calculated as $U_G = 1.871\times10^{-3}$ and $C_G = 2.2$ respectively. The corrected grid uncertainty was $U_{G_c} = 0.663\times10^{-3}$ which is 12.1%D. The corrected grid uncertainty was about 200 times greater than the iterative uncertainty of grid 3 which supports the assumption of neglecting the iterative uncertainty. It should be noted here that the integral variable (which is the total resistance in this case) was not doing oscillations in time vastly because the vessel was not experiencing porpoising. The possible effects of spray (which might also lead to a greater total resistance oscillation in time) were also left out of the study. Due to these reasons, the total resistance reached steady state in time which lead to very low iterative uncertainty, U_I.

r_G refers to grid refinement ratio and is usually taken as $\sqrt{2}$. A finer grid in a three-dimensional flow domain will contain $2\sqrt{2}$ times more elements than the previous grid in a fixed grid system. When the overlapping elements are taken into consideration in the overset grid system the element number will increase even more. Therefore in this study, the grid refinement ratio was taken as $r_G = 1.2$ to limit the number of elements in the fluid domain.

The grid uncertainty was high as compared to those made for fixed grids. This shows that overset grid system requires greater number of elements in the fluid domain and higher computer capability. On the contrary $|E| > U_{G_c}$ in this study which says that the error in computational simulations as compared to the experiments stays within the uncertainty limits and therefore the simulation results were not validated.

The time steps were increased with a refinement ratio of 2. The time step size uncertainty was rather low compared to grid uncertainty. The time step size uncertainty was found to be $U_T = 0.485\times10^{-4}$ which corresponds to 8.8%D. The numerical uncertainty then became $U_N \cong 0.822\times10^{-3}$ which is 14.9%D. Parameters of the grid convergence study are given in Table 4. Details of all these parameters can be found in [18,22].

While evaluating these uncertainty values and parameters of the computational study, it must be noted that an experimental uncertainty study was not available. However, the uncertainty limits of

Table 4
Parameters of the grid convergence study (a), time step convergence study (b).

(a)						
ε_{21}	ε_{32}	R_{G3}	r_G	P_G	δRE_{G3}	C_G
$2.699 * 10^{-4}$	$5.315 * 10^{-4}$	0.506	1.2	3.74	$5.447 * 10^{-4}$	2.2
δ_{G_3}	S	D	U_G	S_c	U_{G_c}	E
$1.208 * 10^{-3}$	$5.837 * 10^{-3}$	$5.487 * 10^{-3}$	34.1%D	$4.629 * 10^{-3}$	12.1%D	15.6%D

(b)				
ε_{21}	ε_{32}	R_{T3}	r_T	U_T
$1.653 * 10^{-4}$	$1.175 * 10^{-4}$	1.407	2	8.8%D

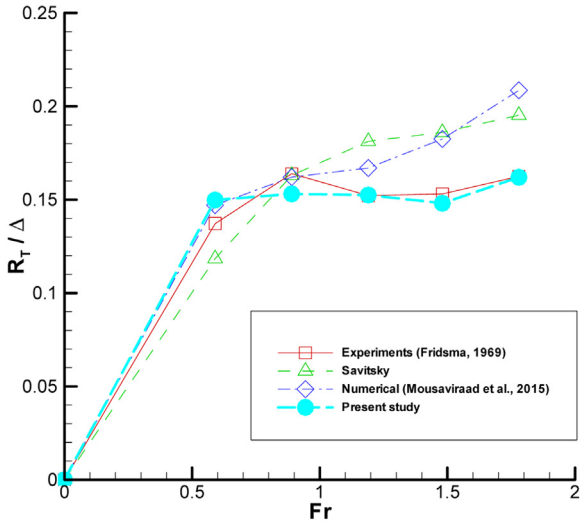

Fig. 5. Calculated resistance characteristics of the Fridsma hull in comparison with experiments, Savitsky method and another RANS-based study.

another high speed vessel whose experiments were conducted in the same towing tank is given in [5].

4. Validation with a benchmark Fridsma hull

The overset grid system was first tested with a prismatic Fridsma hull of $L/B = 4$ and 20° of constant deadrise. The position of LCG is 60%L from the bow and the displacement coefficient is $C_\Delta = 0.608$. The details of the geometry of the hull are given in the reference article (Fridsma, 1969). The resistance characteristics of the hull and the results in comparison with experimental, empirical and numerical studies are given in Fig. 5.

It is seen from Fig. 5 that experiments of Fridsma (1969) were well simulated in this study using the overset grid system. Savitsky empirical approach and the numerical results of Mousaviraad et al. [14] deviate from the experimental results at higher Fr while the agreement is remarkable at all Fr in this study. The trim and sinkage values of the hull are given in Fig. 6.

Calculated trim and sinkage values were in good accordance with the experimental results as depicted in Fig. 6. Although the prediction of the trim angle is somewhat lower than the experimental results at higher Fr, it may be said that the sinkage values were calculated satisfactorily. When the sinkage is correctly predicted, a better estimation of the wetted part of the hull will be obtained which will lead to the estimation of total resistance at a higher precision. The sinkage results of [14] in Fig. 6 indicate that the vessel does not rise above the water as much as in experiments, which leads to higher calculated resistance than experiments given in Fig. 5.

5. Results

Based on experimental and numerical results with rigid body motion and overset grid systems, results were derived in terms of numerical assessment and underlying physics of the planing vessels and the planing regime in general. These outcomes are thoroughly discussed in this section.

5.1. Comparison of numerical results obtained with rigid body motion and overset grid systems

In this section, numerical results obtained with the implementation of rigid body motion and overset grid systems in the fluid domain were compared to investigate their behavior in different Fr numbers.

Fig. 7 represents the total resistance coefficient C_T of the planing hull calculated with different numerical implementations and Savitsky empirical approach in comparison with the experimental data. In this paper, resistance coefficients were non-dimensionalized by;

$$C_x = \frac{2R_x}{\rho S V^2} \tag{12}$$

In this equation subscript x may denote F (friction), P (pressure) or T (total) to represent C_F, C_P and C_T respectively. S is fixed to the wetted surface area of the planing hull in zero forward speed. Fig. 7 reveals that all results are in accordance for $Fr > 0.55$, although it should still be noted that the rigid body motion system predicts slightly less total resistance.

Implementation of the rigid body motion system at lower Fr returns better results when compared with the overset grid system. The rigid body motion system is suitable when the body movement in the flow is restricted because the grid elements are still aligned with the flow. However when the planing hull is subject to large displacements in the flow, the fluid domain is subjected to a large rotation. The hexahedral elements in the fluid domain are getting skewer and the flow is not aligned with the flow anymore. This reflects on the generated results negatively. Fig. 7 (right) shows that the rigid body motion results are getting away from the experiments as the Fr number increases.

The overset grid is flexible to large motions of the planing hull. There is no re-meshing and the elements do not deform. The planing hull is moving together with the grid system around it which makes it consistent in terms of element quality close to its boundaries. Once a high-quality grid system is settled in the fluid domain, the numerical setup will use the same elements to the end of the analysis. The significance of element quality is vital in getting accurate results in CFD which is also reflected to generated resistance values at high Fr numbers in Fig. 7. The overset grid responds quite well when compared with the rigid body motion in terms of the experimental data at high Fr numbers. On the other hand, the error margin is greater at lower Fr. A satisfying conclusion for this is not reached yet as this discrepancy at low Fr with the overset grid needs further investigation.

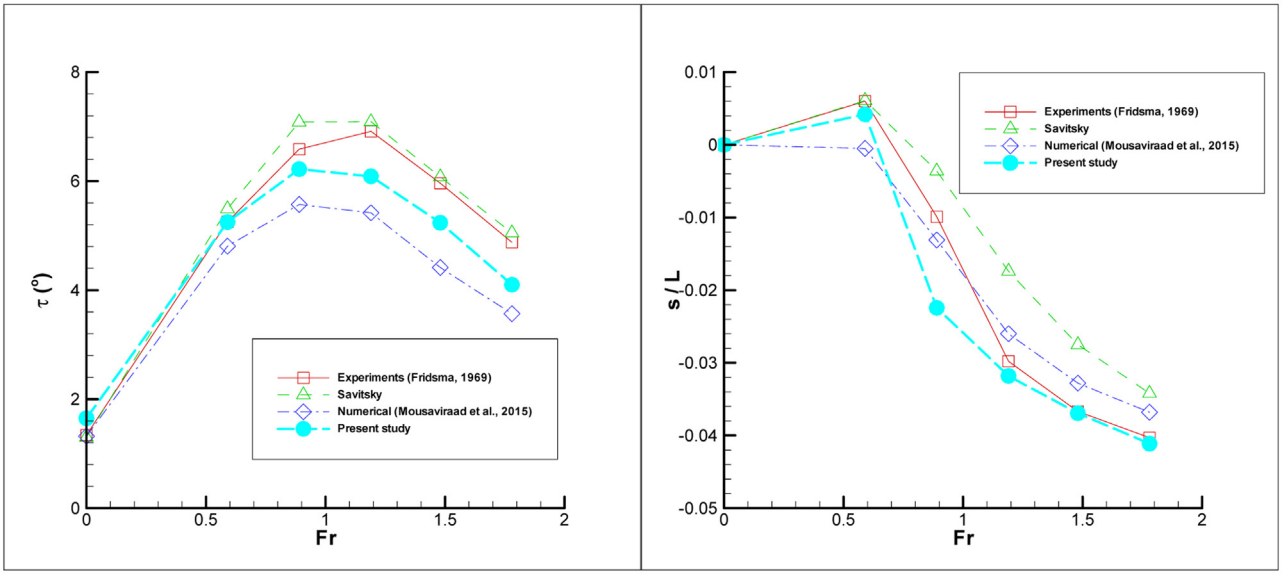

Fig. 6. Trim and sinkage of the Fridsma hull in comparison with experiments, Savitsky method and another RANS-based study.

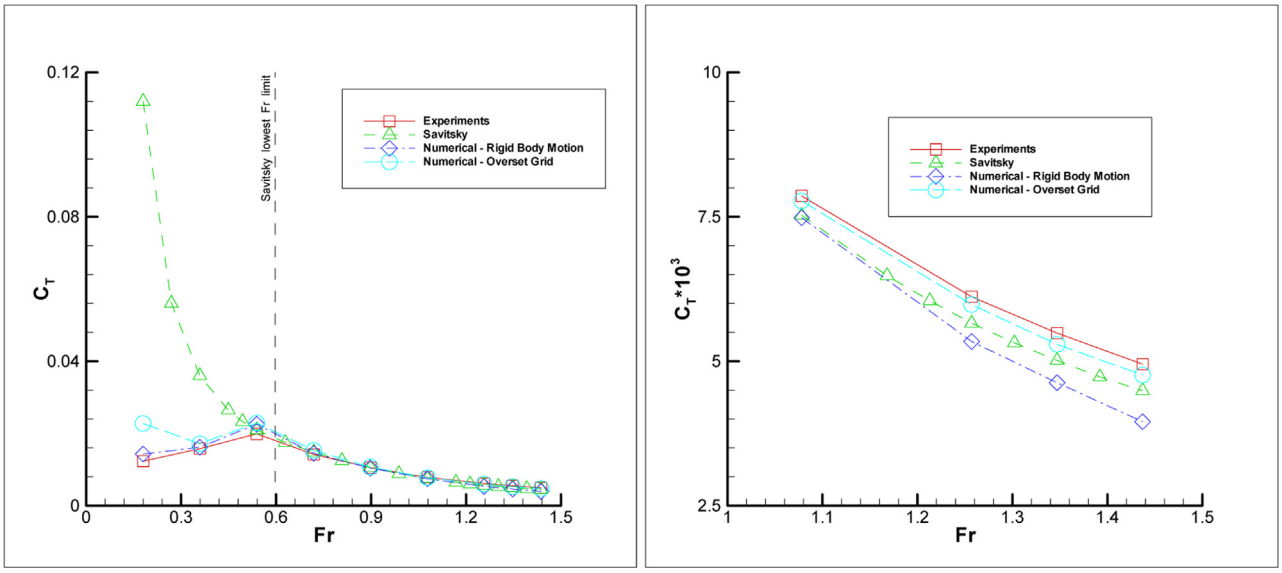

Fig. 7. Comparison of total resistance coefficient, C_T. Numerically generated results versus Savitsky and experiments. The figure on the right provides a zoomed-in version of C_T to evaluate the resistance at higher *Fr* numbers.

The flexibility of the overset grid due to its advantage in modeling large body motions was further investigated with the trim and sinkage response of the planing hull. Fig. 8 reveals the motions of the planing hull at different *Fr* numbers and supports the statements made above for the rigid body motion and overset grid systems. Here, negative sinkage means that the boat goes upward and rises above water while positive sinkage means that the boat sinks in the water. The sinkage was measured from the center of gravity. Small motions of the planing hull were better captured with the rigid body motion while for the larger body motions the overset grid predicted closer results to experiments.

5.2. Decomposition of total resistance

Decomposition of total resistance into its components provides useful information about the characteristics of the body inside the flow. Kinaci et al. [7] have broken down the total resistance into its subparts using CFD to obtain valuable information about resistance characteristics of various forms of bodies, whether submerged or surface-piercing. A similar methodology was adopted in this paper to divide the total resistance into its components to assess a planing hull from hydrodynamical perspective. A comparison will be made with Savitsky approach for separating pressure and frictional resistances to evaluate the accuracy of the empirical approach at the same time. Total resistance is not oscillating significantly in time both experimentally and computationally because the vessel is not experiencing porpoising. However, there are small fluctuations in resistance with respect to time and the resistance values demonstrated in this section are mean values. An example trim and total resistance coefficient history of the planning vessel is given in Fig. 9.

It is of direct notice from Fig. 7 that Savitsky fails to grab the low C_T values of the hull in low *Fr* numbers which should be expected because the empirical approach is valid for planing flow regime covering high *Fr* numbers [15]. At high speeds, whisker spray drag

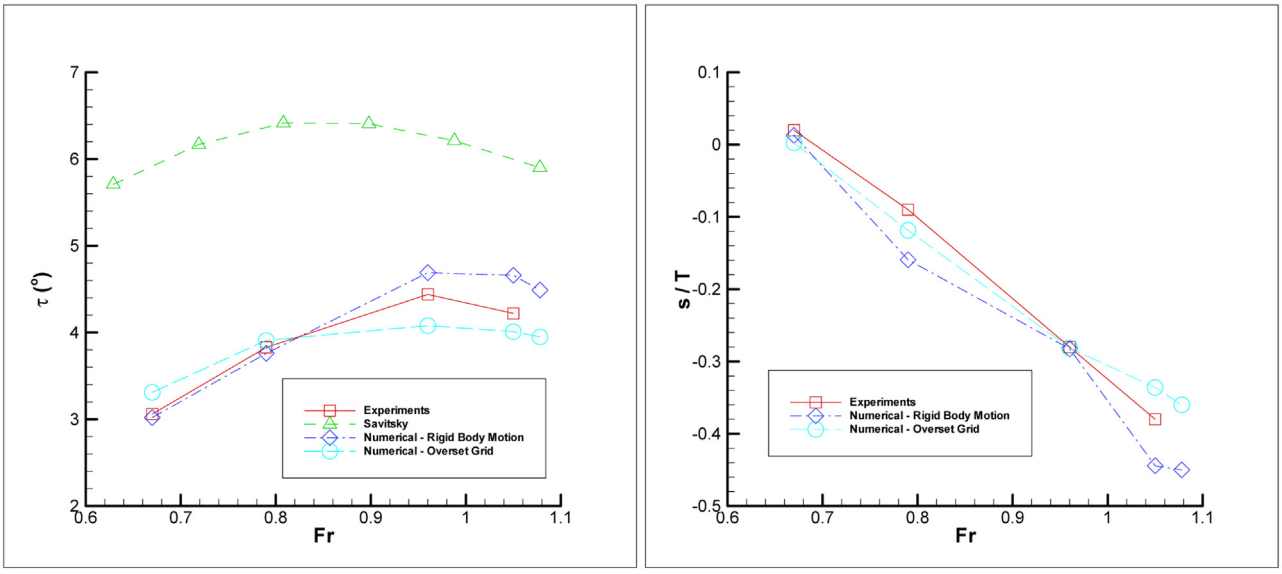

Fig. 8. Trim (left) and sinkage (right) of the planing hull with respect to *Fr*.

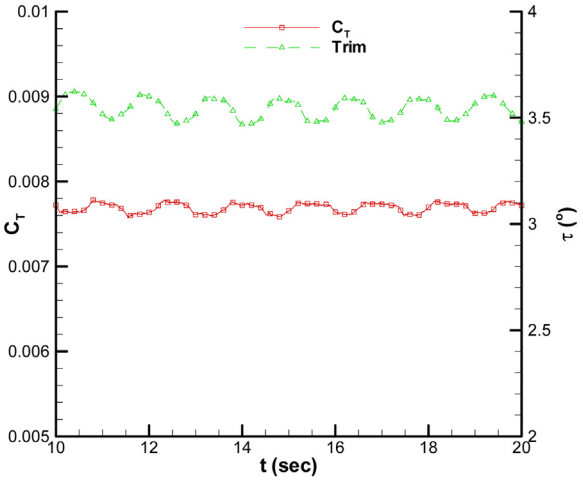

Fig. 9. Trim and total resistance coefficient history of the vessel at $Fr = 0.72$.

Table 5
Comparison of frictional resistance coefficient.

		C_F		
Fr	λ_W	Savitsky	Overset	Difference
0.18	3.583	6.169E-03	3.597E-03	2.573E-03
0.359	3.336	5.146E-03	2.320E-03	2.826E-03
0.539	2.927	4.312E-03	2.592E-03	1.720E-03
0.719	2.472	3.577E-03	2.396E-03	1.181E-03
0.898	2.141	3.058E-03	1.991E-03	1.068E-03
1.078	1.959	2.752E-03	1.724E-03	1.028E-03
1.257	1.858	2.566E-03	1.523E-03	1.043E-03
1.347	1.824	2.497E-03	1.413E-03	1.085E-03
1.437	1.796	2.439E-03	1.387E-03	1.051E-03

also has a significant share in resistance and Savitsky's empirical approach predicts slightly less total resistance compared to the experiments which can be accounted to the exclusion of whisker spray drag. Savitsky (2007) proposed another empirical formula to take into notice the added resistance from whisker spray but in this work it was neglected. He stated that spray drag component can be as much as 15% of the total drag (2007).

Dynamic trim angle predicted by Savitsky given in Fig. 8 is higher at all *Fr* numbers investigated for this case. However, the error margin is greater at lower *Fr* numbers. The large bias of error at this flow regime is the main underlying reason of Savitsky over-predicting the experimental resistance values. Contributions of pressure (C_P) and frictional (C_F) resistances to total resistance predicted by Savitsky are investigated in Fig. 10.

Recalling from the previous sections, the frictional resistance in Savitsky's empirical approach is calculated using Schoenherr's empirical formula which is given in Eq. (5). Based on the experimental data, a general comment about Fig. 10 would be that the pressure resistance is dominant on frictional resistance especially in lower *Fr* numbers. There is a peak at $Fr \approx 0.55$ and after this hump, the significance of pressure resistance in total resistance gradually decreases. This peak points to the transition mode and as the *Fr* increases, the vessel goes into planing mode. In the planing regime, the order of magnitudes of pressure and frictional resistances were about the same.

Another implication of Fig. 10 is that the high degree of error in trim estimation of Savitsky's empirical approach leads to a big discrepancy of pressure resistance in low *Fr* numbers. Savitsky predicts high dynamic trim angles even for really low *Fr*, which substantially increases the predicted total resistance. At these speeds, the planing hull is still in displacement mode high values of pressure resistance are not expected.

Speaking in terms of the resistance coefficients advised by the empirical approach, it should be taken into notice that Savitsky uses Schoenherr's approximation of calculating frictional drag which is actually developed for flat plates. Schoenherr developed his equation for slender bodies. Therefore Schoenherr's formula loses its validity with decreasing λ_W, which is the mean length to beam ratio of the hull. λ_W is calculated by Eq. (3) in Savitsky's approach and for the hull investigated in this study, λ_W values sail around 2–3 which can be examined from Fig. 11.

As the *Fr* number increases, the beam-to-length ratio of the underwater hull increases which leads to the reduction of λ_W with increasing hull speed. As stated before, Schoenherr's formula is given for flat plates which have very large λ_W values. Low values of this parameter will lead results to digress from actual frictional resistance.

Numerical values of C_F obtained empirically (by Savitsky) and numerically (by using overset grid) are given in Table 5. Values

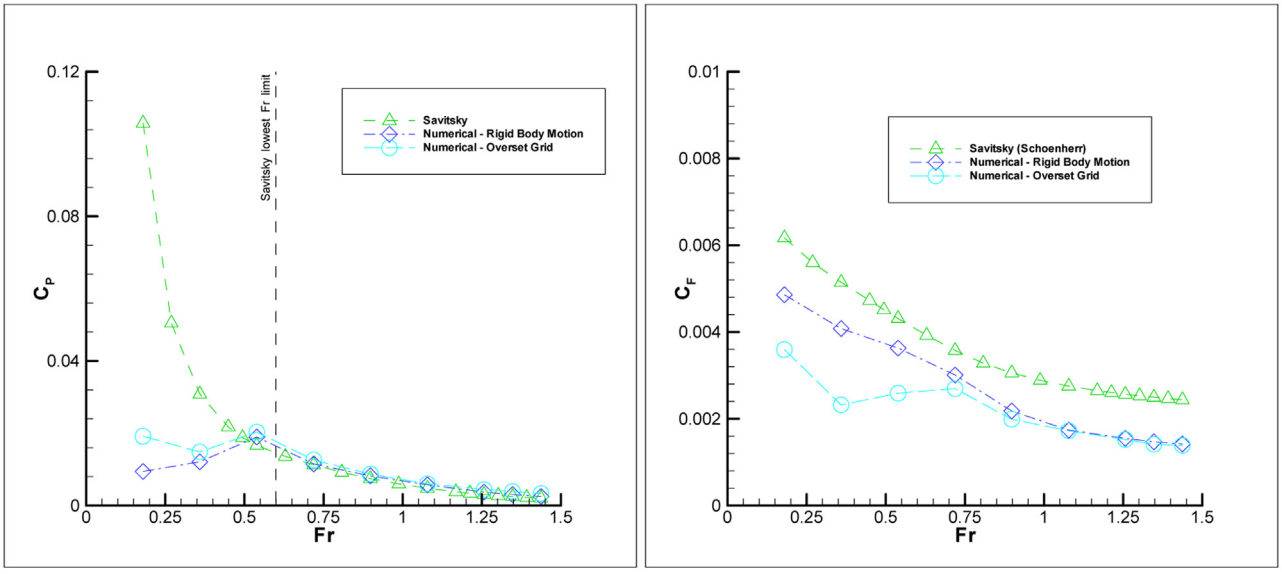

Fig. 10. Pressure (C_P) and frictional (C_F) resistance coefficients calculated numerically and empirically.

calculated by Savitsky were far off from the values given by the overset grid, especially at low *Fr* numbers.

Although in Fig. 10 (right) the difference in C_F may not be well understood, Table 5 points out the fact that Savitsky's C_F values are much higher compared to numerically obtained values in the whole *Fr* number range. In years, CFD has matured and proved its worth in calculating C_F very close to ITTC57 correlation line for displacement ships and there are many papers in the literature that calculate C_F with low error margins. A paper that summarizes all the obtained results for KVLCC2 and KCS displacement hulls for CFD workshop in Gothenburg Larsson et al., 2003 noted the small differences generated by different groups all around the world for frictional resistance. Relying on numerical results for C_F, it can be said that Savitsky approach to calculate the frictional resistance by Schoenherr's formula results in excessive frictional resistance.

5.3. Squat

Fig. 12 reveals the parts of the planing hull under the free surface. The colored parts indicate the part of the hull above the chine. It will be noticed that the underwater parts of the planing vessel at *Fr* = 0.359, *Fr* = 0.539 and *Fr* = 0.67 have bigger volumes compared to the hull at *Fr* = 0.18. This might be unexpected about planing hulls because in normal terms it is expected that the hull rises above water with increasing velocity. However it should be noted that at these *Fr* numbers, the vessel is not in planing regime yet and what happens to the hull at *Fr* = 0.359, *Fr* = 0.539 and *Fr* = 0.67 is *squat*. Squatting is in relation with the flow around the hull and Fig. 13 reveals the non-dimensional flow velocity in the fluid domain at *y* = 0 plane. The velocity is non-dimensionalized by:

$$V' = \frac{V_l}{V_f} \tag{13}$$

Fig. 13 shows the flow velocity for four different cases; *Fr* = 0.18, *Fr* = 0.359, *Fr* = 0.539 and *Fr* = 1.347 respectively. In all of those cases, there is a high velocity and low pressure region under the hull which affects the motion of the vessel in water. At *Fr* = 0.18, this region is close to the bow part of the hull. The vessel orients to the low pressure region which prevents it to lift its bow up the water. Therefore the dynamic trim is limited at this low speed of the hull. At *Fr* = 0.359, the high velocity and low pressure region moves to the stern part of the hull. The low pressure region pulls the aft of

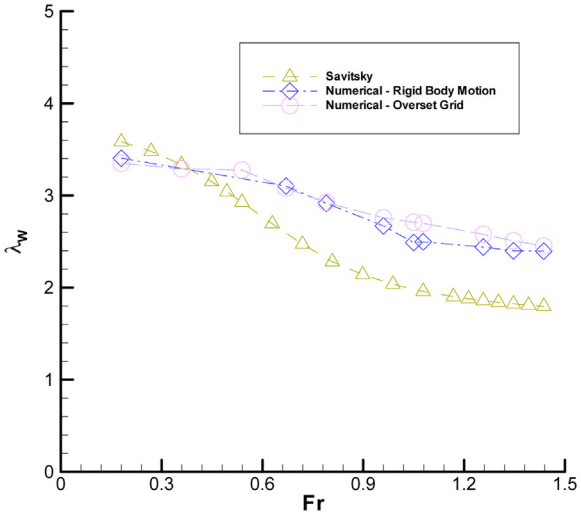

Fig. 11. λ_W values calculated by Savitsky empirical approach and the two numerical approaches.

the ship to contribute to dynamic trim but its effects are still limited due to the distance it has with the bottom of the hull. The region moves to the right and closer to the transom of the hull at *Fr* = 0.539. At this *Fr*, the hull is in transition to planing regime. This region is now very close to the hull and it sinks the stern part of the ship. Although the hull is comparably at a higher *Fr* number, the low pressure region restricts the hull rising above water and getting completely into the planing mode. It contributes to dynamic trim but also leads to squatting. The fourth case is at *Fr* = 1.347 where the hull is completely planing. The high velocity and low pressure region is now past the hull and it does not pull the ship down in water. The hull rises above water and planes in water without any limitations caused by this region.

Squat is related with the low pressure region formed under the hull as revealed by Fig. 13. It moves toward the stern with increasing velocity and pulls the vessel down into water at the transition to planing mode. After this region passes the hull, then the vessel breaks free and starts planing. The non-dimensional free surface elevations in the wake region of the vessel for *Fr* = 0.72 and for *Fr* = 1.347 (in which the vessel is in the planing regime) are given in

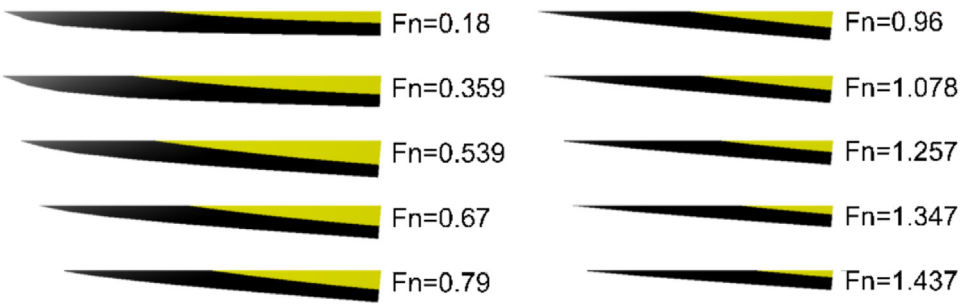

Fig. 12. Part of the planing hull under water at each *Fr*. The different colors represent parts above and below the chine.

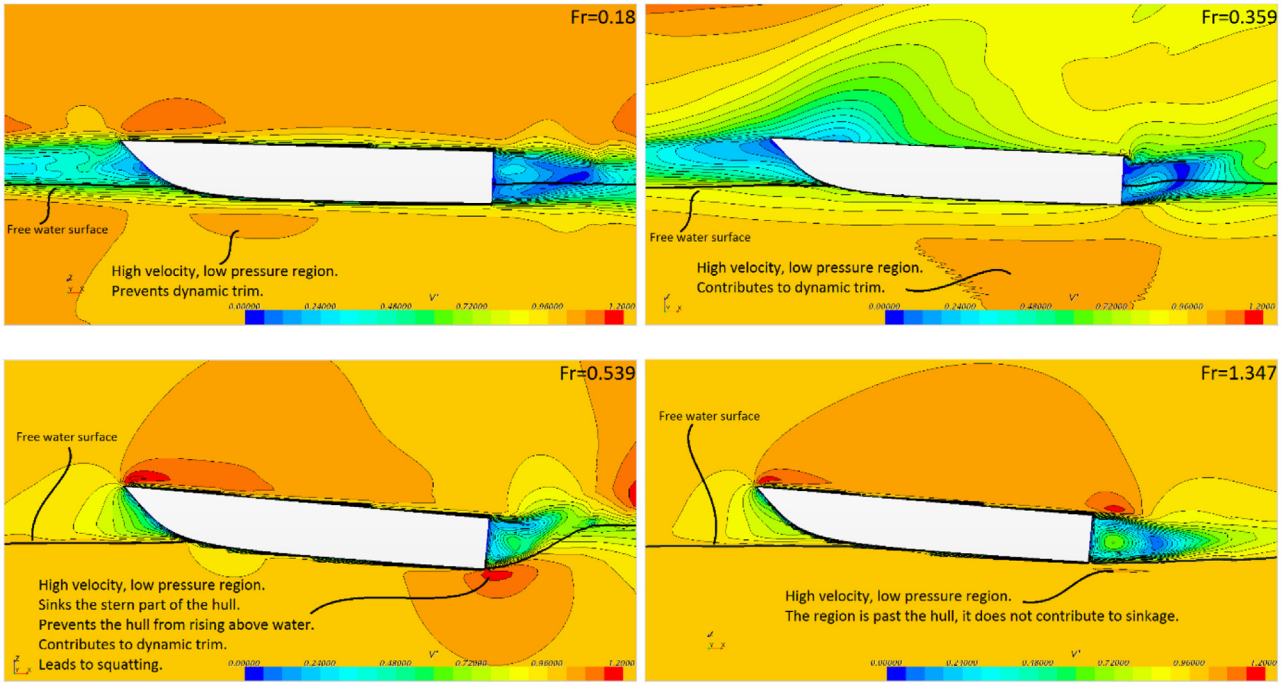

Fig. 13. Non-dimensional flow velocity around the hull at $y = 0$. Above left, $Fr = 0.18$; Above right, $Fr = 0.359$; Below left, $Fr = 0.539$; Below right, $Fr = 1.347$.

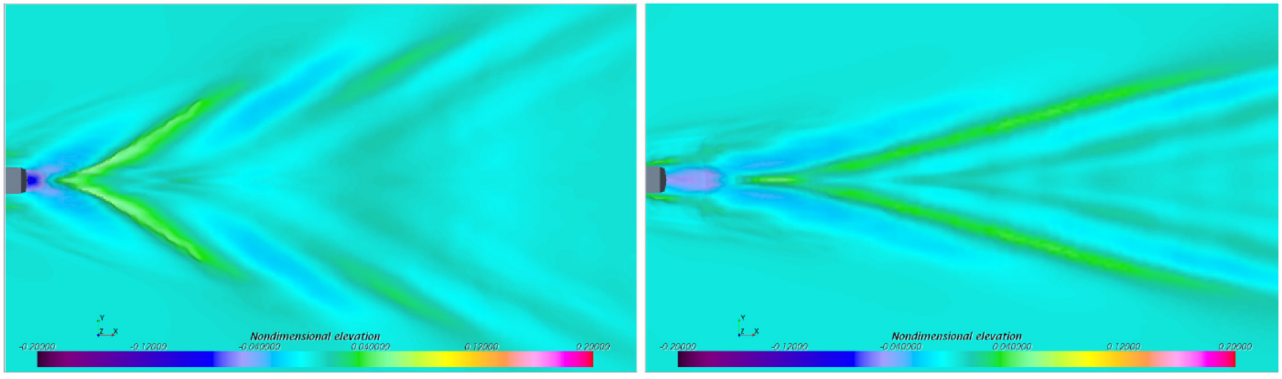

Fig. 14. Non-dimensional free water surface elevations for $Fr = 0.72$ (left) and $Fr = 1.347$ (right).

Fig. 14. The free surface elevations are non-dimensionalized by the length of the vessel.

5.4. Components of lift force on the planing hull

A planing hull with zero forward speed floats in water due to hydrostatic lift (or buoyancy) generated by the fluid. When it starts to move, the geometry of the hull helps generating hydrodynamic lift. The fluid exerts force on the planing hull generating moment about its center of gravity which helps the vessel to rise above water and create dynamic lift. When the hull is in equilibrium in water, the total lift generated by the fluid is equal to its mass times gravity. In short terms it may be said that the total lift force consists of;

$$L = L_{hs} + L_{hd} = W \cdot g \tag{14}$$

Table 6
Decomposition of total lift; hydrostatic and hydrodynamic components at each *Fr*.

Fr	Dynamic Trim (deg)	Sinkage(S/T)	Underwater volume $\left(\frac{\nabla}{LBT}\right)$	Hydrostatic Component $\left(\frac{L_{hs}}{\Delta g}\right)$	Hydrodynamic Component $\left(\frac{L_{hd}}{\Delta g}\right)$
0.18	0	0	0.425	0.997	0.003
0.359	0.94	0.184	0.565	1.327	−0.327
0.579	3	0.193	0.576	1.352	−0.352
0.67	3.31	0.002	0.444	1.041	−0.041
0.79	3.91	−0.119	0.376	0.882	0.118
0.96	4.08	−0.281	0.292	0.686	0.314
1.05	4.01	−0.336	0.256	0.601	0.399
1.078	3.95	−0.356	0.240	0.563	0.437
1.257	3.71	−0.477	0.183	0.431	0.569
1.347	3.47	−0.540	0.152	0.356	0.644
1.437	3.24	−0.592	0.127	0.297	0.703

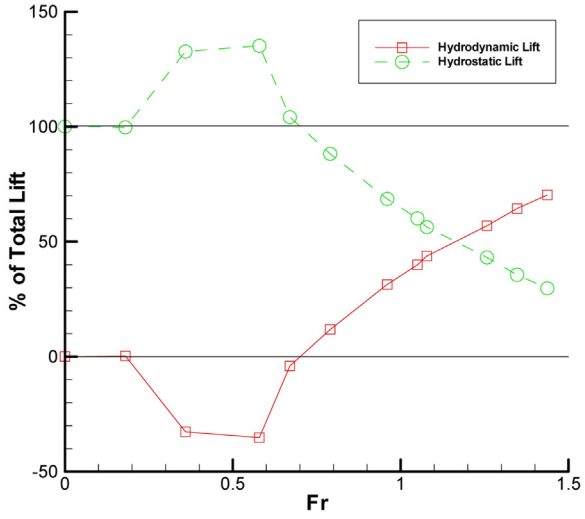

Fig. 15. Graphical presentation of the percentage of lift components vs. *Fr*.

where L_{hs} denotes the hydrostatic lift and L_{hd} represents the hydrodynamic lift. W is the displacement tonnage of the hull and g accounts for gravitation.

It was explained before that the vessel is not experiencing porpoising and the effects of spray were left out of the problem. Therefore at constant speed, the vessel moves steadily and the forces acting on the hull do not experience significant changes in time. It should also be noted that the hydrostatic lift in the case of a planing hull possessing forward motion will be different than that of the hydrostatic lift at zero forward speed. The underwater part of the hull will be changing as expected, and the hydrostatic lift force component is taken as the buoyancy that affects the new part of the underwater hull.

The total lift force calculated numerically can be read from the computed results. As is widely known, hydrostatic lift force is a function of the underwater volume of the hull. By taking into consideration Fig. 12 and calculating the underwater volumes of the planing hull at each *Fr*, hydrodynamic lift force can be calculated using Eq. (14). Following this methodology adopted by Cakici et al. [4], the components of the total lift force along with the underwater volume of the vessel, dynamic trim and sinkage at each *Fr* is given in Table 6. Lift components were non-dimensionalized by the vessel's weight, sinkage by its draft and underwater volume by the rectangular block that surrounds it ($L \times B \times T$).

The graphical presentation of Table 6 is given in Fig. 15. The vessel keeps its position in water with increasing velocity until $Fr = 0.18$ by confronting the required lift to float from hydrostatic force. $0.18 < Fr < 0.67$ is the region where the vessel experiences squat due to decreased pressure in the fluid just below the stern of the vessel. At this flow regime, the hydrostatic lift force increases while the hydrodynamic lift force decreases and goes below zero. Hydrostatic lift force exceeds to meet 100% of the vessel's required total lift to compensate the negative contribution from the hydrodynamic lift component. It might be useful here to refer to Fig. 13 to understand why the hydrodynamic force attains negative values. Hydrostatic lift force reaches up to 135% of the total required lift at $Fr = 0.579$ where the sinkage makes its peak. Figs. 7 and 10 implicitly show the peak in sinkage which actually reveals the point of highest total resistance coefficient and pressure coefficient.

Hydrodynamic lift force becomes a real contributor of total lift after $Fr > 0.67$ and raises the boat above water. The increase in hydrodynamic lift is sharp at the beginning and this increase is more gradual as the *Fr* number increases. Hydrostatic lift force is still the major component of total lift up to $Fr \approx 1.1$. After that point, it can be said that the vessel is totally in planing mode.

6. Conclusions

Based on the arguments in this study, following conclusions were made:

- Overset grid system results were in better accordance with the experiments in high *Fr* while rigid body motion system results were better in low *Fr*. Rigid body motion system is not suitable for large motions of the hull due to flow misalignment.
- Savitsky approach implementing Schoenherr's formula returns high frictional resistance in the whole *Fr* number range. The method also generates very high pressure resistance at low *Fr* numbers where the hull is in the displacement mode. The reason for this is that Savitsky proposed his empirical approach to assess a planing hull in terms of total resistance at high velocities where the vessel is in planing mode. Although Savitsky's method generates close total resistance results for a planing hull, the components of total resistance were not calculated with enough accuracy. Therefore if the resistance components of a planing hull are to be evaluated, it would be misleading to rely on Savitsky's empirical approach.
- The flow regime where the vessel faces squat was identified with computational visualization. It is shown that the low pressure region in the flow moves backward with increasing *Fr* number. When this low pressure region is close to the stern of the hull, it pulls the vessel down and also contributes to dynamic trim. The vessel sinks inside water increasing the total resistance. The region where squat takes place in the whole *Fr* number range was identified by the negative hydrodynamic lift contribution of the hull. It was found that significant squat occurs around $0.2 < Fr < 0.7$ for this vessel.

Research on clear identification of flow modes of a planing vessel is still ongoing. There is still work on computation of wave resistance of a planing hull and it is considered that a more detailed

breakup of total resistance into its components will help reveal the intrinsic nature of the planing regime.

Acknowledgments

The authors acknowledge the support of Gozuyilmaz Engineering & Marine Industries Ltd. for this work to be prepared. The authors are especially grateful to Mr. Ozgur Inam for granting the access to publish the experimental data, Mr. Cihad Delen from ITU for his helps in explanation of lab setup and Prof. Sakir Bal for his valuable comments on this study.

References

[1] S. Bal, S. Kinnas, A numerical wave tank model for cavitating hydrofoils, Comput. Mech. 32 (December) (2003) 259–268.
[2] S. Bal, High-speed submerged and surface piercing cavitating hydrofoils, including tandem case, Ocean Eng. 34 (October) (2007) 1935–1946.
[3] S. Bal, et al., 30 knot Motorboat Model Experiments and Analyses (Report No. 2014-Gozuyilmaz-P05-M393), 2014.
[4] F. Cakici, O.F. Sukas, O. Usta, A.D. Alkan, A computational investigation of a planing hull in calm water by U-RANSE approach, International Conference on Advances in Applied and Computational Mechanics (2015).
[5] C. Delen, S. Bal, Uncertainty analysis of resistance tests in ata nutku ship model testing laboratory of istanbul technical university, J. Marit. Mar. Sci. 1 (December (2)) (2015) 8–27.
[6] H. Ghassemi, S. Yu-min, Determining the hydrodynamic forces on a planing hull in steady motion, J. Mar. Sci. Appl. 7 (September) (2008) 147–156.
[7] O.K. Kinaci, O.F. Sukas, S. Bal, Prediction of wave resistance by a Reynolds-averaged Navier-Stokes equation-based computational fluid dynamics approach, Proc. Inst. Mech. Eng. Part M: J. Eng. Marit. Environ. 230 (June (3)) (2016) 531–548.
[8] A.R. Kohansal, H. Ghassemi, M. Ghaisi, Hydrodynamic characteristics of high speed planing hulls, including trim effects, Turk. J. Eng. Environ. Sci. 34 (October) (2010) 155–170.
[9] A.R. Kohansal, H. Ghassemi, A numerical modeling of hydrodynamic characteristics of various planing hull forms, Ocean Eng. 37 (April) (2010) 498–510.
[10] P. Lotfi, M. Ashrafizaadeh, R.K. Esfahan, Numerical investigation of a stepped planing hull in calm water, Ocean Eng. 94 (January) (2015) 103–110.
[11] K.I. Matveev, Hydrodynamic modeling of planing hulls with twist and negative deadrise, Ocean Eng. 82 (May) (2014) 14–19.
[12] K.I. Matveev, Hydrodynamic modeling of semi-planing hulls with air cavities, Int. J. Naval Arch. Ocean Eng. 7 (May) (2015) 500–508.
[13] M.G. Morabito, Empirical equations for planing hull bottom pressures, J. Ship Res. 58 (December (4)) (2014) 185–200.
[14] S.M. Mousaviraad, Z. Wang, F. Stern, URANS studies of hydrodynamic performance and slamming loads on high-speed planing hulls in calm water and waves for deep and shallow conditions, Appl. Ocean Res. 51 (June) (2015) 222–240.
[15] D. Savitsky, Hydrodynamic design of planing hull, Mar. Technol. 1 (1) (1964) 71–95.
[16] D. Savitsky, M.F. DeLorme, R. Datla, Inclusion of whisker spray drag in performance prediction method for high-speed planing hulls, Mar. Technol. 44 (January (1)) (2016) 35–56.
[17] D. Savitsky, M. Morabito, Surface wave contours associated with the forebody wake of stepped planing hulls, Mar. Technol. 47 (January (1)) (2010) 1–16.
[18] F. Stern, R.V. Wilson, H.W. Coleman, E.G. Paterson, Comprehensive approach to verification and validation of CFD simulations –Part 1: methodology and procedures, J. Fluids Eng. –Trans. ASME 123 (December (4)) (2001) 793–802.
[19] Star CCM+ Documentation, Version 10.02, CD-Adapco, 2015.
[20] S.T.G. Veysi, M. Bakhtiari, H. Ghassemi, M. Ghiasi, Toward numerical modeling of the stepped and non-stepped planing hull, J. Braz. Soc. Mech. Sci. Eng. 37 (November (6)) (2015) 1635–1645.
[21] S. Volpi, H. Sadat-Hosseini, M. Diez, D.H. Kim, F. Stern, R. Thodal, J. Grenestedt, Validation of high fidelity CFD/FE FSI for full-scale high-speed planing hull with composite bottom panels slamming, Proceedings of the 4th International Conference on Coupled Problems in Science and Engineering (2015).
[22] R.V. Wilson, F. Stern, H.W. Coleman, E.G. Paterson, Comprehensive approach to verification and validation of CFD simulations –Part 2: application for RANS simulation of a Cargo/Container ship, J. Fluids Eng. –Trans. ASME 123 (4) (2001) 803–810.
[23] R. Yousefi, R. Shafaghat, M. Shakeri, Hydrodynamic analysis techniques for high-speed planing hulls, Appl. Ocean Res. 42 (August) (2013) 105–113.
[24] O.M. Faltinsen, Hydrodynamics of High Speed Marine Vehicles, Cambrige University Press, UK, 2005.